ELSEVIER

Journal of Power Sources 90 (2000) 163–169

JOURNAL OF POWER SOURCES

www.elsevier.com/locate/jpowsour

Improvement of thermal cycle characteristics of a planar-type solid oxide fuel cell by using ceramic fiber as sealing material

S. Taniguchi [a,*], M. Kadowaki [b], T. Yasuo [a], Y. Akiyama [a], Y. Miyake [b], K. Nishio [a]

[a] *New Material Research Center, SANYO, Co., Ltd., 1-1 Dainichi-higashimachi, Moriguchi, Osaka 570-8502, Japan*

[b] *Heating, Refrigeration and Energy Development Center, SANYO Co., Ltd., 1-1-1 Sakata, Oizumi-cho, Oura-gun, Gumma 370-0596, Japan*

Received 11 August 1999; received in revised form 24 November 1999; accepted 19 February 2000

Abstract

The objective of this paper is to improve the endurance of solid oxide fuel cell (SOFC) against thermal cycles by reducing the stress caused by the difference in thermal expansion coefficients of alloy separator and electrolyte. The thermal cycle characteristics were improved by using a ceramic fiber for the sealing material. The ceramic fiber seemed to play the role of suppressing electrolyte-cracking by relaxing the stress set up during thermal cycles. The appropriate structure for the sealing material was investigated with 200 mm × 150 mm × 4 combined-cell single-layer modules. The glass was arranged around the internal manifold to suppress gas leakage, and the ceramic fiber was arranged around the electrolyte to prevent the glass from contacting the electrolyte. It was confirmed that the thermal cycle characteristics can be improved and that good cell performance can be maintained by adopting this gas seal structure.

Keywords: Solid oxide fuel cell; Thermal cycle; Sealing material; Structure

1. Introduction

Solid oxide fuel cells (SOFCs) provide advantages of high energy conversion efficiency, such as heat utilization and the ability to utilize a variety of fuels, due to their high operating temperature. They are expected to become a major electric power source in the future. Planar-type SOFCs are superior to those having tubular designs because of their simple manufacturing process and the promise of a higher power density. For the separator material, a heat-resistant alloy offers better performance than $LaCrO_3$-based ceramics in terms of heat conductivity, ease of manufacturing and mechanical strength. Furthermore, it does not have the problem of volume instability in the reducing atmosphere of the anode that is associated with $LaCrO_3$-based ceramics [1,2].

The authors fabricated a 2-kW SOFC module that has a combined-cell structure with a nickel-based austenitic alloy for the separator [3]. However, it exhibited bad thermal cycle characteristics. The electrolyte was broken from the sealing part by a thermal cycle. This seemed to be caused by stress due to the difference in thermal expansion coefficients of the separator and the electrolyte, and the problem must naturally become worse with a large-scale system.

Heat-resistant ferritic alloys, which have a lower thermal expansion coefficient than nickel-based austenitic alloys, were investigated for the separator material with a 50 × 50 mm single cell [4]. The thermal cycle characteristics were improved, but the improvement was insufficient because the electrolyte cracked was after a repetition of thermal cycles. The electrolyte cracked from the area in contact with the sealing material of a glass plate.

In this paper, the objective is to improve endurance against thermal cycles by reducing the stress caused by the difference in thermal expansion coefficients of the separator and the electrolyte. In Section 3.1, the effect of improving thermal cycle characteristics by using a ceramic fiber was investigated with 150 × 150 mm single-layer cells. In Section 3.2, the appropriate structure for the sealing material is investigated with 200 × 150 mm × 4 combined-cell single-layer modules.

* Corresponding author. Fax: +81-6-6900-3556.
E-mail address: s_taniguchi@rd.sanyo.co.jp (S. Taniguchi).

0378-7753/00/$ - see front matter
PII: S0378-7753(00)00405-5

2. Experimental

2.1. Investigation of improving thermal cycle characteristics by using ceramic fiber

The specifications of the sealing materials in this study are presented in Table 1. The glass plate was made up of an alkaline earth borosilicate glass (SiO_2, 49 wt.%; BaO, 25 wt.%; B_2O_3, 15 wt.%; Al_2O_3, 10 wt.%; As_2O_3, 1 wt.%; Na_2O, 0.3 wt.%) with a softening temperature of 1108 K, a thermal expansion coefficient of 4.6×10^{-6}/K, and a thickness of 0.40 mm. A commercially available non-crystal silica/alumina (SiO_2, 52 wt.% + Al_2O_3, 48 wt.%) fiber (FIBERFRAX® FFX paper #300, Toshiba Monofrax) was used for the ceramic fiber. The average diameter of the fiber was 2.5 μm and its bulk density was 0.3 g/cm^3. The thickness measured at room temperature with tightening pressure of 2 kgf/cm^2 was 0.35 mm. The glass/YSZ mixture was made of a borosilicate glass (SiO_2, 80 wt.%; B_2O_3, 13 wt.%; Al_2O_3, 2 wt.%; Na_2O, 4 wt.%; K_2O, 1 wt.%) (particle size, $d = 1$ μm), 60 wt.% + YSZ (8 mol% Y_2O_3 + 92 mol% ZrO_2) ($d = 0.5$ μm), 40 wt.%. The thickness of the glass/YSZ mixture was 0.10 mm.

The specifications of the cells and modules in this study are presented in Table 2. A schematic diagram of the 150×150 mm cell structure is presented in Fig. 1. Cell performances by using the glass plate and the ceramic fiber for the sealing material were investigated with 150×150 mm single-layer cells A and B. Sealing materials for A and B were arranged as shown in Fig. 2. The glass plate described above was used for the sealing material of A. The ceramic fiber was put on the separator side and the glass/YSZ mixture was put on the electrolyte side for the sealing material of B. The width of the sealing material was 5 mm.

The cell components were constructed as follows. The separators were made of Inconnel 600 (Cr 18 wt.%, Fe 8 wt.%, Ni Bal.) with a thermal expansion coefficient of 16.7×10^{-6}/K. The electrolyte was made up of PSZ (3 mol% Y_2O_3 + 97 mol% ZrO_2) and had a size of 150×150 mm and a thickness of 200 μm. The electrolyte has holes for the internal manifold. The anode material, which consisted of NiO ($d = 1$ μm), 56 wt.% + YSZ, 44 wt.%, was painted on the surface of the electrolyte. The electrode area was 130 cm^2. $La_{0.8}Sr_{0.2}MnO_3$ ($d = 1$ μm), 80 wt.% + YSZ ($d = 0.5$ μm), 20 wt.%, was used for the cathode material. It was painted on the other side and then sintered at 1573 K for 2 h. $La_{0.9}Sr_{0.1}MnO_3$ ($d = 1$ μm), 90 wt.% + La_2O_3 ($d = 0.5$ μm), 10 wt.%, was used for the cathode's second layer material and was painted on the cathode. This layer plays the role of suppressing the chromium diffusion from the alloy separator to the cathode. $La_{0.9}Sr_{0.1}CoO_3$ ($d = 1$ μm) was used as the material of the cathode's current-collecting layer and was painted on the cathode's second layer. The total thickness of the cathode, the cathode's second layer and the cathode's current-collecting layer was 0.34 mm. Nickel felt was used for the anode's current collector. The total thickness of the anode and the anode's current collector was estimated at 0.35–0.40 mm under the operating conditions of 1273 K reducing atmosphere and tightening pressure of 2 kgf/cm^2.

A and B were operated at 1273 K with air for the cathode gas and hydrogen for the anode gas. The tightening pressure of the cells during operation was 2 kgf/cm^2. Fuel utilization and oxidant utilization were changed by varying the gas flow rate.

In the thermal cycle test, the cell was cooled from 1273 K to room temperature and then heated from room temperature to 1273 K at a speed of 100 K/h while supplying nitrogen to the anode instead of hydrogen.

2.2. Investigation of appropriate structure for sealing material with combined-cell single layer-modules

Fig. 3 shows a schematic diagram of the 2-kW combined-cell stacked module. The sizes of the separator and unit cell are 350×350 mm and 200×150 mm, respectively. Four unit cells are arranged on the separator in each layer. Sealing materials are arranged around each cell. The appropriate structure for the sealing material was investigated with combined-cell single-layer modules C and D that have the same structure as shown in Fig. 3. Fig. 4 shows a schematic diagram of the gas seal structures for C and D. The same materials as described in Section 2.1 were used for the glass plate, the ceramic fiber and the glass/YSZ mixture. Suppression of electrolyte-cracking during thermal cycle while maintaining high gas seal efficiency was attempted for D by using both the glass and the ceramic fiber. For suppressing gas leakage through the sealing material, the separator was designed so that the width of the sealing material was increased to 7 mm and the entire area of the sealing material was pressed by both sides of the separator. The appearance of D is shown in Fig. 5.

Table 1
Specification of sealing materials in this study

	Material	Thickness (mm)
Glass plate	Alkaline earth borosilicate glass plate	0.40
Ceramic fiber	Silica/alumina ceramic fiber (SiO_2 52 wt.% + Al_2O_3 48 wt.%)	0.35[a]
Glass/YSZ mixture	Borosilicate glass 60 wt.% + YSZ powder 40 wt.%	0.10

[a] Thickness measured at room temperature and with tightening pressure of 2 kgf/cm^2.

Table 2
Specifications of cells and modules in this study

	A	B	C	D
Size	150 × 150 mm		200 × 150 mm × 4 cell	
Type	Single-layer cell		Combined-cell single-layer module	
Sealing material	Glass plate	Ceramic fiber + glass/YSZ mixture	Ceramic fiber + Glass/YSZ mixture	Glass plate + ceramic fiber + glass/YSZ mixture

A PSZ plate with a size of 200 × 150 mm and a thickness of 0.20 mm was used for the electrolyte of C. It covered the internal manifold area and had holes for the internal manifold. A YSZ plate with a size of 146 × 150 mm and a thickness of 0.30 mm was used for the electrolyte of D. It did not cover the internal manifold area. A PSZ plate with a thickness of 0.62 mm was put over the internal manifold area and was expected to act as an electric insulator. The PSZ plate had holes for the internal manifold. In the case of D, in which the electrolyte was separated from the internal manifold area, it became possible to use YSZ because it exhibits higher ionic conductivity and lower strength than PSZ for the electrolyte.

The electrode area of the unit cell of C and D was 162.5 cm^2. Other conditions were the same as those described in Section 2.1.

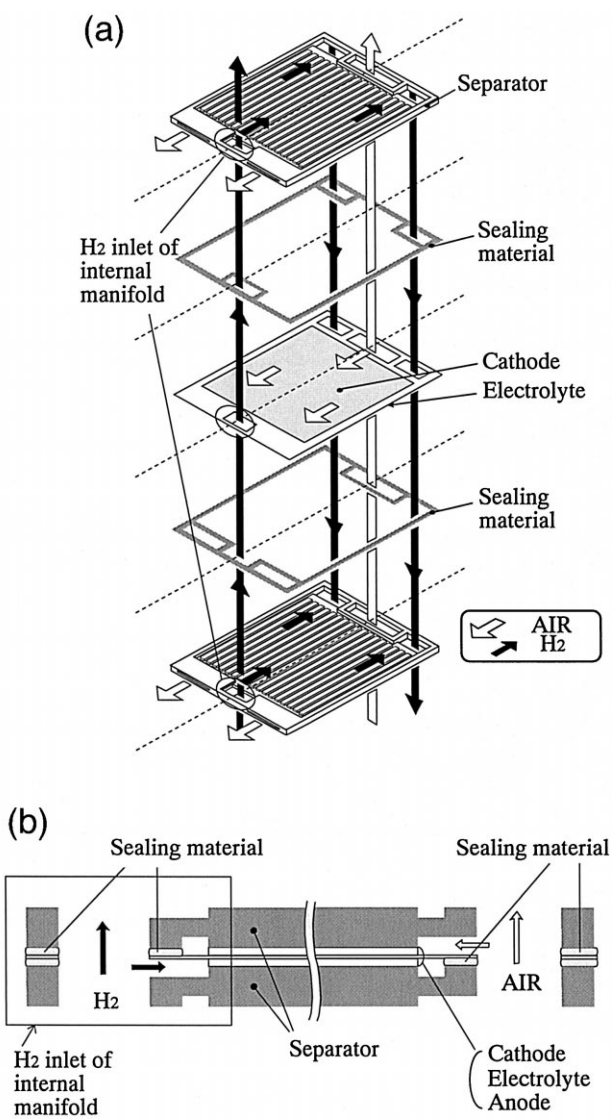

Fig. 1. Schematic diagram of 150×150 mm cell structure.

3. Results and discussion

3.1. Investigation of improving thermal cycle characteristics by using ceramic fiber

Fig. 6 shows the change in cell voltage at 0.3 A/cm^2 by a repetition of thermal cycles for A and B. The cell performance of A greatly degraded after one thermal cycle. After the cell test of A, it was found that the electrolyte was broken from the area in contact with the glass. This seemed to be caused by the stress due to the difference between the thermal expansion coefficients of the separator (16.7×10^{-6}/K) and the electrolyte (11×10^{-6}/K). This stress is believed to be generated and increased after the glass solidified and connected the separator and the electrolyte in the cooling process.

On the other hand, cell performance degradation by thermal cycles was small for B even after 12 thermal

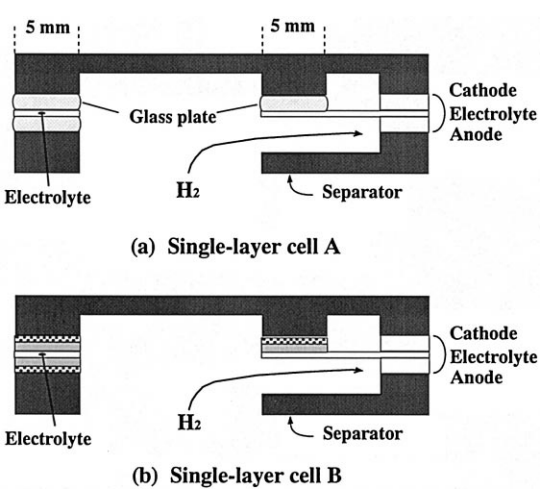

Fig. 2. Schematic diagram of gas seal structure at H_2 inlet of internal manifold for 150×150 mm single-layer cells A and B.

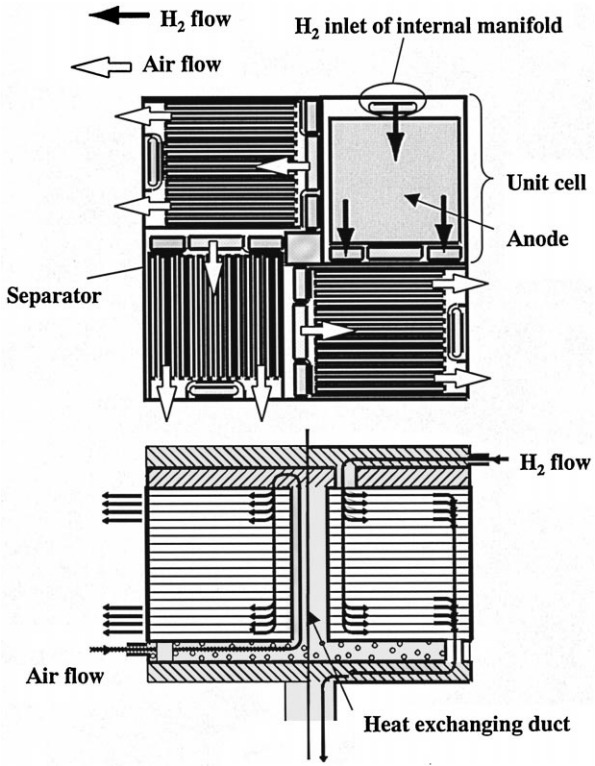

Fig. 3. Schematic diagram of combined-cell stacked module.

cycles. Fig. 7 shows the relationship between the cell voltage of B and current density for the number of thermal cycles. After the cell test of B, no crack was found in the electrolyte. The ceramic fiber seemed to play the role of

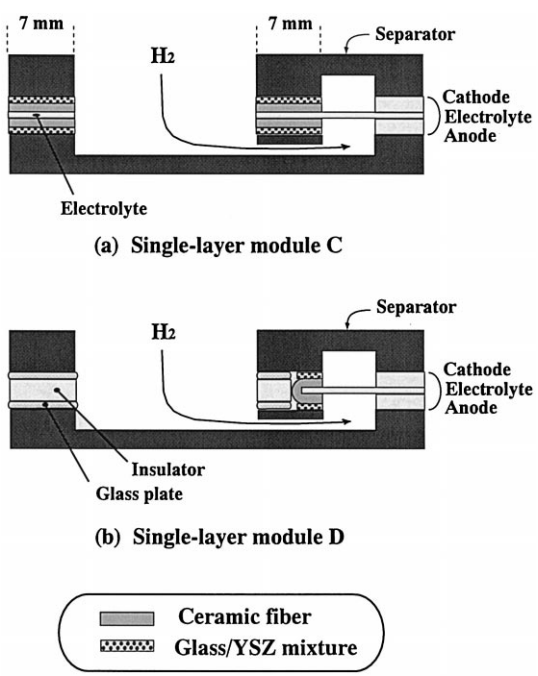

Fig. 4. Schematic diagram of gas seal structures at H_2 inlet of internal manifold for combined-cell single-layer modules C and D.

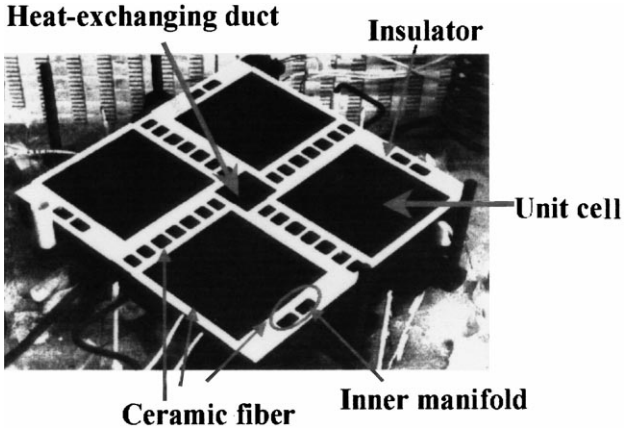

Fig. 5. Appearance of combined-cell single-layer module D.

suppressing electrolyte-cracking by relaxing the stress set up during thermal cycles.

Fig. 8 shows the change in cell voltage by fuel utilization and oxidant utilization for A before the thermal cycle and for B after four thermal cycles. Even at relatively low levels of fuel utilization and oxidant utilization, the cell voltage of B was lower than that of A. Furthermore, the cell voltage drop of B with increasing fuel utilization and oxidant utilization was larger than that of A. It seemed that for B, the effective electrode area decreased due to gas leakage and generation of H_2O near the sealing material. The gas leakage was believed to have occurred through the ceramic fiber because the gas seal property for the glass/YSZ mixture had been confirmed as sufficient by the authors.

From the above results, it was confirmed that the thermal cycle characteristics were improved by using the ceramic fiber for the sealing material. However, gas seal property of the ceramic fiber was not sufficient. On the other hand, the glass exhibited a better gas seal property although it broke the electrolyte during the thermal cycle. Then, a method of improving the thermal cycle characteristics while maintaining a high gas seal efficiency was investigated as described below.

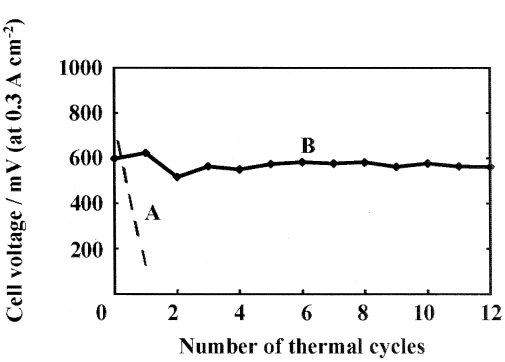

Fig. 6. Change in cell voltage for A and B by thermal cycles. Fuel utilization was 20% and oxidant utilization was 40% at 0.3 A/cm^2.

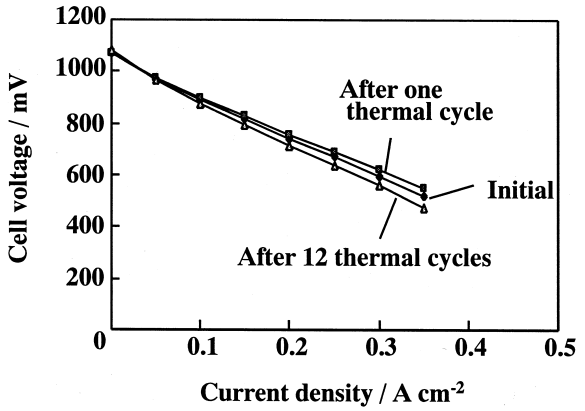

Fig. 7. Relationship between the cell voltage of B and the current density for number of thermal cycles. Fuel utilization was 20% and oxidant utilization was 40% at 0.3 A/cm^2.

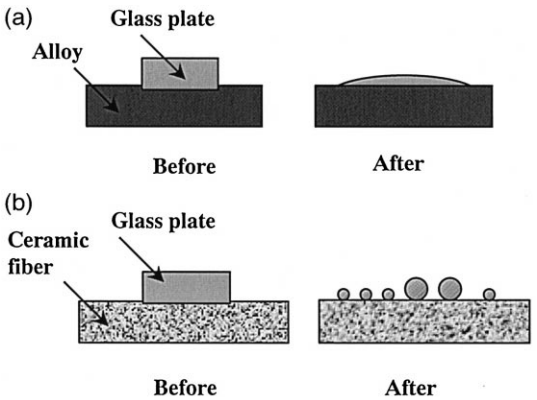

Fig. 9. Schematic diagram of contact between glass and alloy (a) and between glass and ceramic fiber (b) before and after a thermal cycle.

3.2. Investigation of appropriate structure for sealing material with combined-cell single-layer modules

In order to observe the state of contact between the cell components and to investigate a method to suppress cracking of the electrolyte, thermal cycle tests for the cell components were performed. In this test, the cell components were heated from room temperature to 1273 K and then cooled from 1273 K to room temperature in air at a speed of 100 K/h. The state of contacts between the glass plate and the separator and that between the glass plate and the ceramic fiber were observed before and after a thermal cycle. The results are presented schematically in Fig. 9. Fig. 9(a) indicates that the separator was wetted by the glass under the operating conditions and that the glass spread on the separator. This means that the glass would spread and likely come in contact with the electrolyte under the operating conditions even if the glass were not in contact with the electrolyte during fabrication. Fig. 9(b) indicates that the ceramic fiber was only slightly wetted by the glass under the operating conditions.

From the above results, the structure for the sealing materials, as shown in Fig. 4(b), was devised. The glass was arranged around the internal manifold to suppress gas leakage. An insulator made up of PSZ with a thickness of 0.62 mm was attached to the internal manifold area. The insulator exhibited high strength because of its thickness, and was expected to endure the stress. In order to prevent glass from contacting the electrolyte, the ceramic fiber was arranged around the electrolyte.

In order to confirm the effect of suppressing electrolyte-cracking by this structure, cell components, arranged as shown in Fig. 10, were subjected to a thermal cycle. In Fig. 10(a), the electrolyte broke from the edge where it made contact with the glass. On the other hand, no crack was found in Fig. 10(b). This was apparently due to the

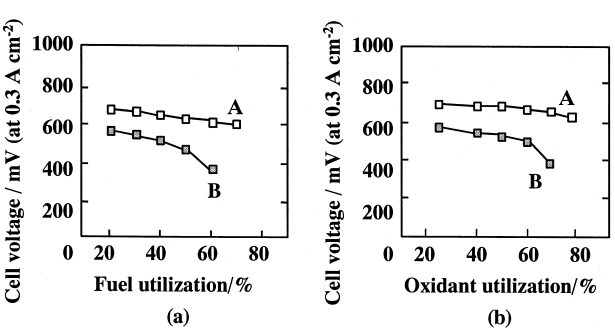

Fig. 8. Change in cell voltage by fuel utilization and oxidant utilization for A and B.

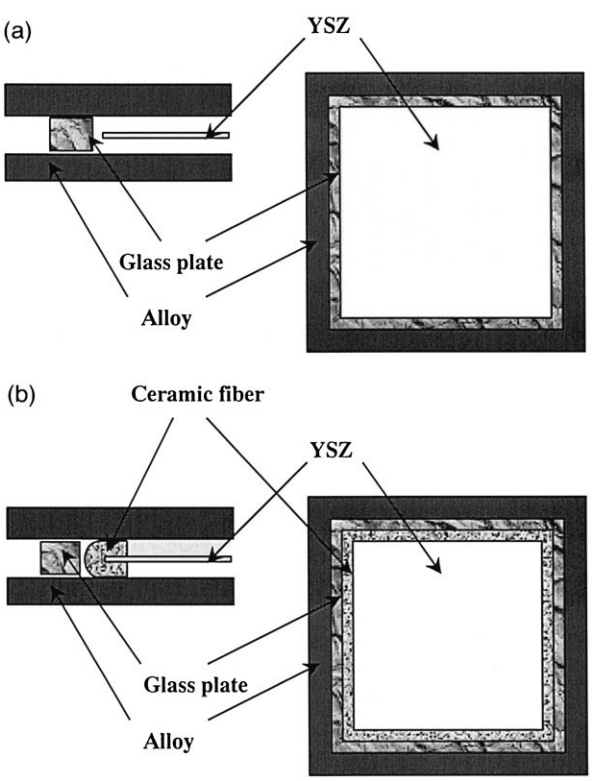

Fig. 10. Arrangement of cell components in thermal cycle test to confirm effect of suppressing electrolyte-cracking.

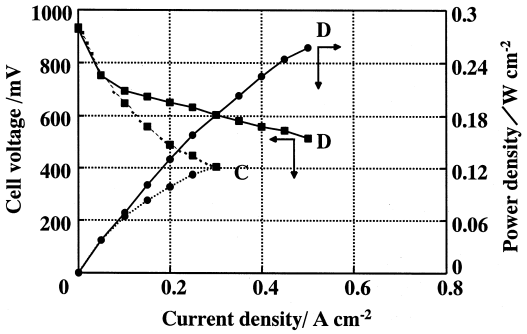

Fig. 11. Relationships among cell voltage, current density and power density for C and D at constant fuel utilization of 65% and oxidant utilization of 10%.

ceramic fiber being arranged around the electrolyte, which prevented the electrolyte from contacting the glass.

Fig. 11 shows the relationship between cell voltage, current density and power density for C and D at constant fuel utilization of 65% and oxidant utilization of 10%. The cell voltage of C at 0.3 A/cm^2 was 404 mV and the power density was 0.12 W/cm^2. The cell voltage of D at 0.5 A/cm^2 was 515 mV and the power density was 0.26 W/cm^2. The cell performance of D was better than that of C. Fig. 12 shows the relationships among cell voltage, current density and power density for D at constant fuel utilization of 70% and oxidant utilization of 10%. The cell voltage was 546 mV at 0.4 A/cm^2 and the power density was 0.22 W/cm^2.

Fig. 13 shows the change in cell voltages by fuel utilization. The cell voltage of C was a little higher than that of B at high fuel utilization. This improvement seemed to be caused by the gas seal structure of C, in which the width of the sealing material was increased and the entire sealing material was pressed by both sides of the separator. However, the cell performance of C was insufficient. The cell voltage of D was higher than C by about 200 mV at 0.3 A/cm^2, a difference larger than the value calculated from the ionic conductivities of YSZ and PSZ (about 90

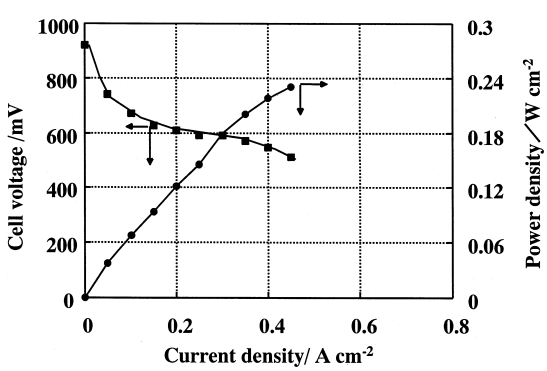

Fig. 12. Relationships among cell voltage, current density and power density for D at constant fuel utilization of 70% and oxidant utilization of 10%.

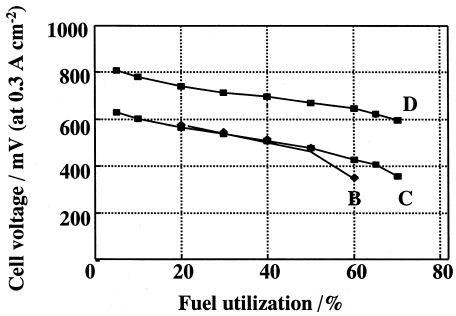

Fig. 13. Change in cell voltage by fuel utilization for B, C and D.

mV at 0.3 A/cm^2). Figs. 14 and 15 show the change in open circuit voltage by gas flow rates. In these figures, the horizontal axis is the ratio of the gas flow rate and that of the calculated gas flow rate under the conditions of 100% gas utilization at 0.3 A/cm^2. The change in open circuit voltage by fuel flow rate was almost the same for C and D. On the other hand, the open circuit voltage of C lowered remarkably with decreasing oxidant flow rate, while it remained a high value for D. This means that the oxygen partial pressure in the cathode of C became significantly lower with decreasing oxidant flow rate. Thus, the gas seal property for D improved more than for C.

After the cell performance measurement, the modules were cooled to room temperature and taken apart into pieces. The states of the cathode's and anode's current collectors of C indicated that gas leakage was remarkable around the internal manifold and fuel gas leaked to the cathode side. It seemed that fuel leaked to the cathode side in the case of C, while gas leakage was suppressed by arranging the glass around the internal manifold in the case of D. As shown in Fig. 3, hydrogen inlet and air outlet of the internal manifold are placed side by side, and hydrogen outlet and air inlet of the internal manifold are also placed side by side. The glass around the internal manifold, in the case of D, prevented gas leakage between hydrogen inlet and air outlet, and between hydrogen outlet and air inlet. This seemed to be the cause of the improvement of gas seal property for D.

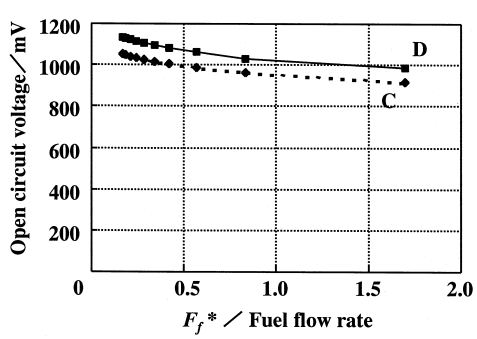

Fig. 14. Change in open circuit voltage for C and D by fuel flow rate. F_f^*: calculated fuel flow rate under conditions of 100% fuel utilization at 0.3 A/cm^2. F_{OX}^* /oxidant flow rate = 16.5%.

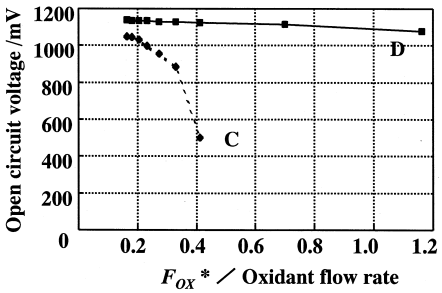

Fig. 15. Change in open circuit voltage for C and D by oxidant flow rate. F^*_{OX}: calculated oxidant flow rate under conditions of 100% oxidant utilization at 0.3 A/cm^2. $F_f{}^*$ /fuel flow rate = 16.8%.

The electrolytes of C and D did not have the type of break near the sealing part that was observed in A. It was found , however, that there were a few cracks in the electrolytes of C and D, unlike B. The cracks seemed to be caused by stress due to the volume expansion of the nickel felt used as the anode's current collector by oxidation in the cooling process. It was found that the oxidation of the nickel felt in C and D gradually occurred from outside of the combined cell, and it seemed that the stress set up in the electrolyte must be non-uniform, which would explain the electrolyte-cracking. Therefore, it seems that reducing this kind of stress is necessary in the future.

As a result, it was confirmed that the thermal cycle characteristics can be improved by using ceramic fiber as the sealing material and that good cell performance can be maintained by adopting the gas seal structure of the combined-cell single-layer module D.

4. Conclusions

The thermal cycle characteristics were improved by using a ceramic fiber for the sealing material. The ceramic fiber seemed to play the role of suppressing electrolyte-cracking by relaxing the stress set up during thermal cycles. It was also confirmed that good cell performance can be maintained with 200 × 150 mm × 4 combined-cell single-layer modules by adopting the gas seal structure in which the glass was arranged around the internal manifold to suppress gas leakage, and the ceramic fiber was arranged around the electrolyte to prevent glass from contacting the electrolyte.

Acknowledgements

This work was performed as an R&D program of the New Energy and Industrial Technology Development Organization (NEDO) under the New Sunshine Project of the Agency of Industrial Science and Technology, MITI.

References

[1] I. Yasuda, M. Hishinuma, Proc. Int. Symp. Solid Oxide Fuel Cells (SOFC-IV) 4 (1995) 924.
[2] P.H. Larsen, P.V. Hendriksen, M. Mogensen, J. Therm. Anal. 49 (3) (1997) 1263.
[3] Y. Akiyama, T. Yasuo, S. Taniguchi, M. Kadowaki, Y. Miyake, K. Nishio, in: Proc. of the 6th FCDIC Fuel Cell Symposium, 1996, p. 195.
[4] S. Taniguchi, M. Kadowaki, T. Yasuo, Y. Akiyama, Y. Miyake, K. Nishio, Denki Kagaku 65 (1997) 574.